PCCP

Accepted Manuscript

This article can be cited before page numbers have been issued, to do this please use: M. Baranac-Stojanovi and M. Stojanovi, *Phys. Chem. Chem. Phys.*, 2019, DOI: 10.1039/C8CP07875K.

This is an Accepted Manuscript, which has been through the Royal Society of Chemistry peer review process and has been accepted for publication.

Accepted Manuscripts are published online shortly after acceptance, before technical editing, formatting and proof reading. Using this free service, authors can make their results available to the community, in citable form, before we publish the edited article. We will replace this Accepted Manuscript with the edited and formatted Advance Article as soon as it is available.

You can find more information about Accepted Manuscripts in the author guidelines.

Please note that technical editing may introduce minor changes to the text and/or graphics, which may alter content. The journal's standard Terms & Conditions and the ethical guidelines, outlined in our author and reviewer resource centre, still apply. In no event shall the Royal Society of Chemistry be held responsible for any errors or omissions in this Accepted Manuscript or any consequences arising from the use of any information it contains.

ROYAL SOCIETY OF CHEMISTRY

rsc.li/pccp

The Effect of the Two Types of Dibenzoannulation of Pentalene on Molecular Energies and Magnetically Induced Currents

View Article Online
DOI: 10.1039/C8CP07875K

Marija Baranac-Stojanović[a]* and Milovan Stojanović[b]

[a] *University of Belgrade - Faculty of Chemistry, Studentski trg 12-16, P.O.Box 158, 11000 Belgrade, Serbia*

e-mail: mbaranac@chem.bg.ac.rs

[b] *University of Belgrade, Institute of Chemistry, Technology and Metallurgy - Center for Chemistry, Njegoševa 12, P.O.Box 473, 11000 Belgrade, Serbia*

Abstract

The effect of two ways of dibenzo-fusion of pentalene, in singlet and triplet states, on molecular energies and magnetically induced ring currents was examined by density functional calculations. The isomerization energy decomposition analysis (IEDA), along with the calculated aromaticity indices ($NICS(1)_{zz}$, HOMA and FLU_{π}), estimation of resonance energies (RE) and extra cyclic resonance energies (ECRE) by NBO method, and the NICS-*XY*-scans revealed that the π-electronic system is the most important factor controlling molecular energies. The [*a*,*f*] topology features greater delocalization which results in two opposing effects: larger ECRE, but weaker π-bonding. The latter is mainly responsible for higher energy of [*a*,*f*]-dibenzopentalene (DBP) (ΔE_{iso} = 21.7 kcal/mol), other effects being σ-orbital and electrostatic interactions. The reversal of energetic stability in triplet states (ΔE_{iso} = −10.8 kcal/mol) mainly comes from reduced Pauli repulsion in [*a*,*f*]-DBP, which stabilizes the unpaired spin density over the central trimethylenemethane subunit vs the central pentalene subunit in [*a*,*e*]-DBP. While [*a*,*e*] topology only reduces diatropic and paratropic currents of elementary subunits, benzene and pentalene, the [*a*,*f*] one creates strong global paratropicity involving benzene rings, as well. Both DBP isomers are characterized by global and smaller semi-global and local diatropic currents in triplet state.

1. Introduction

View Article Online
DOI: 10.1039/C8CP07875K

The cyclic π-electron conjugation can stabilize or destabilize a molecule, with respect to appropriate reference, which depends on the number of π-electrons. If the number is (4n+2), the system is stable and aromatic, as proposed by Hückel.[1] Conversely, when the number of π-electrons is 4n, the system is unstable and antiaromatic, as suggested by Breslow and co-workers.[2] The concepts of aromaticity and antiaromaticity have long been attracting a great deal of attention from theoretical and synthetic chemists, though the latter concept mainly from theoretical chemists due to experimantal inaccessibility of antiaromatic compounds.[3] Pentalene, which is composed of two fused cyclopentadiene rings, belongs to this latter class of compounds. It has 8π-electrons and is unstable above –196 °C,[4] but can be stabilized by formation of organometallic species,[5] within non-IPR fullerenes,[6] electronically, by annulation to aromatic rings, or sterically.[7] Polycycles, composed of (4n+2)π-electron and 4nπ-electron rings can display properties of both aromatic and antiaromatic compounds, which depends on molecular topology. This makes them interesting in the field of material chemistry. For example, arene-annulated pentalenes emerged as promising candidates for applications in organic and molecular electronics.[7,8]

The simplest member of diarene-annulated pentalene is dibenzopentalene (DBP), which appears in two isomeric forms differing in the position of the fused benzene ring (Figure 1). The first synthesis of the [*a*,*e*]-fused skeleton was achieved by Brand in 1912,[9] whereas the parent compound was obtained by Blood and Linstead in 1952.[10] In this molecule, the otherwise antiaromatic pentalene attains conjugated diene properties[10] and the recent theoretical studies showed weak paratropicity of the pentalene core[11,12] and nonaromaticity of the two five-membered rings.[12] Diareno[*a*,*e*]pentalene scaffold has become a target of a number of synthetic chemists[8,13] which is due to its intriguing electronic properties, where a possibility to create stable compounds with controllable antiaromaticity is of particular interest for the development of new organic electronic materials.[14]

View Article Online
DOI: 10.1039/C8CP07875K

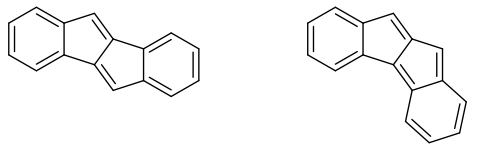

Dibenzo[*a*,*e*]pentalene Dibenzo[*a*,*f*]pentalene

Figure 1. Two isomers of dibenzopentalene.

The isomeric [*a*,*f*]-type topology had been known only in dianionic[15] and dihydro-forms[8e,15b] until recently when Konishi, Yashuda and co-workers synthesized the first dibenzo[*a*,*f*]pentalene derivative.[16] It showed C_s symmetry, which was also predicted before by theoretical calculations,[17] appreciable open-shell singlet character in its ground state and small singlet-triplet energy gap.[16] They were explained to be a consequence of increased antiaromaticity due to the π-electron delocalization initiated by resonance of the *ortho*-quinoidal structure of one benzene ring.[16] The experimental ^{1}H NMR chemical shifts and calculated NICS(1), NICS(1)$_{zz}$ and HOMA values for individual rings supported enhanced antiaromaticity which involved benzene rings, too.[16] Hence, the previuosly predicted strong paratropic current for [*a*,*f*]-isomer, which extended beyond the pentalene subunit and encompassed one benzene ring,[11a] has been borne out by the recent experimental data.

The position of benzene ring fusion, obviously, creates significant differences in electronic structures of the two isomeric dibenzopentalenes and the related molecular properties. Whereas the most basic ones have been disclosed in ref. 16, the fundamental question about the relative energy of the isomers and factors controlling it is still unanswered. Thus, it is the purpose of this paper to give an insight into the energetics of the two species, in both singlet and the first excited triplet states, to identify factors which determines their relative energies and also to examine how antiaromaticity of the ground state of [*a*,*f*]-isomer changes upon excitation into the triplet state. The triplet state of [*a*,*e*]-isomer was examined before[12] and will be analyzed herein as a comparison to the [*a*,*f*]-isomer. Investigation and rationalization of isomer dependent properties has been a

View Article Online
DOI: 10.1039/C8CP07875K

research topic of many scientists.[12,14a,18] This kind of information provides us the fundamental chemical knowledge and allows us to explain or predict basic properties of related systems.

2. Computational Details

Molecular geometries were optimized employing the Gaussian 09 program package[19] at the B3LYP/6-311+G(d,p) level of theory.[20] The restricted and unrestricted models were used for closed-shell singlet and open-shell triplet calculations, respectively. Since the RB3LYP wave function was unstable in the case of [*a*,*f*]-DBP this compound was also treated by the unrestricted broken-symmetry (BS) method which results in open-shell singlet species and represents an alternative to computationaly more demaning multiconfigurational or multireference methods.[21] Spin contamination is $\langle S^2 \rangle = 0.46$ for C_s symmetric structure and $\langle S^2 \rangle = 0.55$ for C_{2v} symmetric structure. Frequency calculations, which were run immediately after the optimizations, confirmed the nature of stationary points as minima, no imaginary frequency, or transition state structure having one imaginary frequency. The source of energy difference between [*a*,*e*]- and [*a*,*f*]-isomers, in their singlet and triplet states, as well as between different electronic states of the same compound, was explored by the dissection of the relative energy into contributions from deformation and interaction energy, where the latter was further decomposed into five energy components with the aid of the localized molecular orbital energy decomposition analysis (LMOEDA) of Su and Li,[22] which is implemented in the Gamess program package.[23] The details of the analysis are given in the Results and Discussion section.

The (anti)aromaticity was analyzed by the structural harmonic oscillator model of aromaticity (HOMA) index,[3i,24] the aromatic fluctuation index (FLU_π)[25] and the magnetic $NICS(1)_{zz}$ index.[26] The HOMA index allows an assessment of the degree of bond length alternation (BLA) in a molecule and is based on the fact that aromatic systems show a tendency toward bond length equalization, while antiaromatic ones contain alternating single and double bonds. The HOMA values close to one indicate little or no BLA, that is a delocalized (aromatic) system, while negative

View Article Online
DOI: 10.1039/C8CP07875K

values and those close to zero denote a localized (antiaromatic) system or weakly delocalized (nonaromatic) system, respectively. The FLU_π index is the measure of the fluctuation of π-electronic charge between adjacent atoms in a given ring and is based on the fact that aromatic systems are characterized by an extensive electron delocalization. It takes into account not only the amount of electrons shared between two atoms, but also the similarity of electron sharing between adjacent atoms. Its values close to zero indicate π-electron delocalization and aromaticity, while they increase in the case of nonaromatic and antiaromatic molecules. The HOMA and FLU_π were calculated for mono-, di- and tricycles as subunits of the studied molecules, as well as for molecular perimeter. Thus, they give information about local, semi-global and global electron delocalization. These indices were calculated by using the Multiwfn program.[27] The FLU_π data were obtained for closed-shell species, only. The $NICS(1)_{zz}$ index corresponds to the out-of-plane component of magnetic shielding calculated 1 Å above the center of the ring. Its negative values denote diatropic currents and aromaticity, while positive values indicate paratropic currents and antiaromaticity. The $NICS(1)_{zz}$ values were obtained by the GIAO method[28] at the (U)B3LYP/6-311+G(d,p) level of theory. In addition to the single NICS value, the magnetically induced currents were analyzed by the NICS-*XY*-scans which can identify the type of local, semi-global and global currents and are important for systems composed of fused (4n+2) and 4nπ-electron subunits that can develop both diatropic and paratropic currents. The NICS-*XY*-scans were performed at the same level of theory as the single NICS calculations by using the Aroma 1.0 package. The scans were recorded 1.7 Å above the plane of the molecule and include only the π-electron contributions by employing the σ-only model.[29]

The resonance energy (RE) due to π-electron delocalization was estimated on the basis of second order perturbative analysis of donor-acceptor interactions between natural bond orbitals (NBO). This analysis gives an estimate of energy lowering ($\Delta E^{(2)}_{ij}$) due to the interactions between occupied and empty orbitals and is calculated as shown in Eq. 1, where q_i is the occupancy of donor

View Article Online
DOI: 10.1039/C8CP07875K

orbital, F_{ij} refers to the strength of orbital interactions and E_j and E_i are the respective orbital energies.[30] For the purpose of this analysis the NBO 6.0,[31] linked to the Gaussian 09, was used.

$$\Delta E^{(2)}_{ij} = -q_i|F_{ij}|^2/ E_j - E_i \quad (1)$$

3. Results and Discussion

3.1. Relative energies of singlet and triplet states

Calculated relative energies of [*a*,*e*]-DBP and [*a*,*f*]-DBP in their singlet and triplet states are shown in Figure 2. In the most stable open-shell singlet state, the [*a*,*f*]-isomer is by 21.4 kcal/mol higher in energy than [*a*,*e*]-DBP. The closed-shell state of [*a*,*f*]-DBP is destabilized by only 0.3 kcal/mol relative to its open-shell singlet state. Both structures have C_s symmetry. Increase in symmetry to C_{2v} results in the triplet ground state, the energy of which is between that of open-shell and closed-shell singlet species, by 0.1 kcal/mol above the open-shell singlet. These results agree with the experimentally observed easy thermal singlet-triplet excitation.[16] Both open-shell and closed-shell C_{2v} singlet states contained one imaginary frequency (–1461.2 cm^{-1} and –1258.7 cm^{-1}, respectively), the vibrational mode of which showed tendency for symmetry reduction. This means that the two C_s singlet structures could rapidly equilibrate over the C_{2v} transition states, as also proposed in ref. 16, with the low barriers of 1.8 kcal/mol for open-shell singlet and 2.5 kcal/mol for closed-shell singlet. Therefore, due to very small energy differences, various electronic states of [*a*,*f*]-DBP should readily interconvert. By contrast, the [*a*,*e*]-DBP is a closed-shell species with the triplet state being 32.3 kcal/mol higher in energy.

Calculated bond lengths (Table S1) and ^{1}H NMR chemical shifts (Table S2) are in good agreement with experimental data obtained for dibenzo[*a*,*f*]pentalene derivative[16] and point to the C_s ground state.

View Article Online
DOI: 10.1039/C8CP07875K

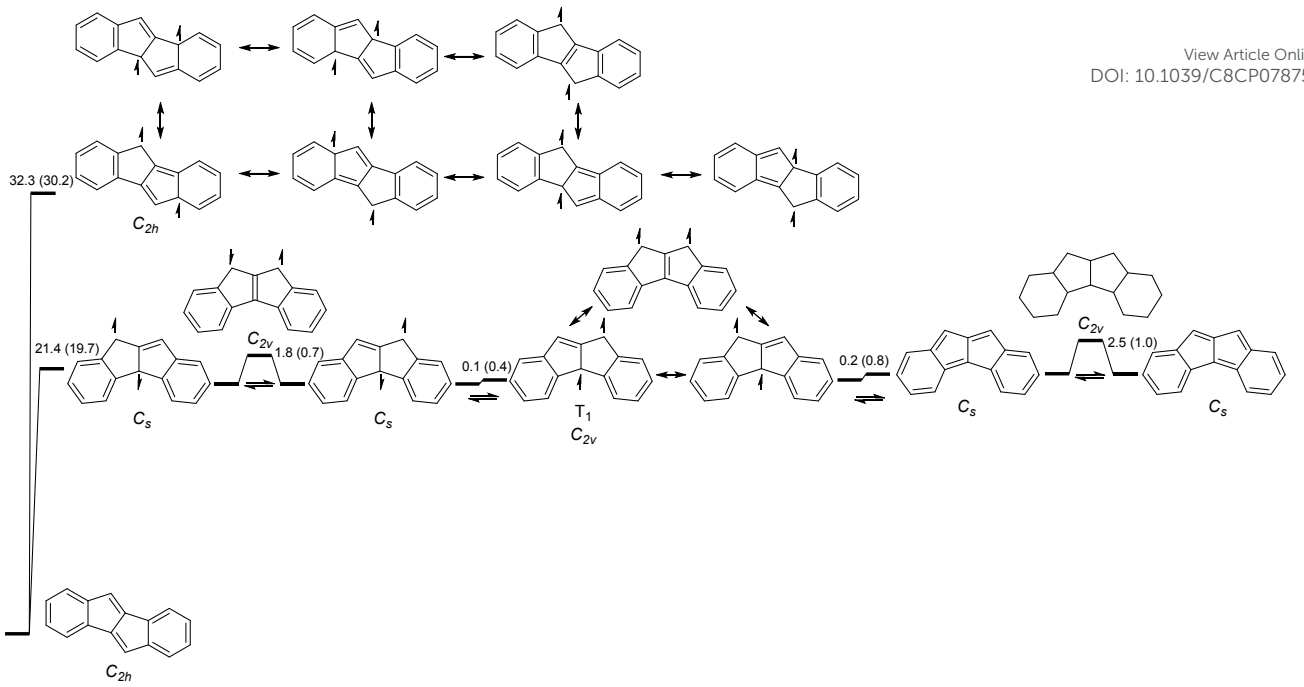

Figure 2. Relative energies (in kcal/mol) of dibenzo[*a*,*e*]pentalene and dibenzo[*a*,*f*]pentalene in their singlet and triplet states. Values in brackets include zero point energy.

The spin density analysis (Table S3) shows that the unpaired spin density of singlet and triplet [*a*,*f*]-DBP is mainly distributed over the trimethylenemethane subunit (Figure 2), as also estimated previously,[16] whereas in triplet [*a*,*e*]-DBP it is distributed over the whole pentalene subunit (Figure 2).

3.2. Singlet states of dibenzopentalenes

After the successful synthesis of [*a*,*f*]-DBP derivatives by Konishi, Yashuda and co-workers, the [*a*,*f*]-DBP core was described as highly antiaromatic.[16] Does antiaromaticity destabilize [*a*,*f*]-DBP relative to [*a*,*e*]-DBP?

3.2.1. Resonance energy and extra cyclic resonance energy

Since antiaromaticity means that the cyclic π-electron delocalization does not stabilize molecule with respect to an acyclic structural analogue, we first estimated the total π-electron

View Article Online
DOI: 10.1039/C8CP07875K

delocalization energy, or resonance energy, of [*a*,*e*]-DBP and [*a*,*f*]-DBP in its closed-shell and open-shell singlet states by summing up stabilizing energies of all individual $\pi \rightarrow \pi^*$ interactions. The, thus obtained, total delocalization energy amounts 370.0 kcal/mol for [*a*,*e*]-DBP, 367.3 kcal/mol for closed-shell [*a*,*f*]-DBP, 190.4 kcal/mol and 204.0 kcal/mol for alpha and beta spin orbitals of open-shell singlet [*a*,*f*]-DBP, or a total of 394.4 kcal/mol for the latter. Hence, the obtained quantitative data support large π-electron delocalization in the open-shell singlet [*a*,*f*]-DBP, whereas the two closed-shell species are similarly stabilized by resonance. Now, to evaluate the effect of cyclic delocalization on molecular stability the resonance energy of an appropriate acyclic reference system should be subtracted from the obtained values. It has been shown previosly that the most suitable acyclic reference molecules are those having the same number and the same type of π conjugations as in cyclic molecule and the associated energy was termed as extra cyclic resonance energy (ECRE).[18b,32] The smallest conjugated subunit in both DBP isomers is 1,3-butadiene, so we used this reference to evaluate (de)stabilization arising from cyclic delocalization. Butadiene can adopt two planar conformations, *cis* and *trans*, where the former benefits 25.6 kcal/mol from π-electron delocalization and the latter 30.2 kcal/mol, according to our calculations. The [*a*,*e*]-DBP has eight *cis*-butadiene conjugations and three *trans*-butadiene conjugations, while [*a*,*f*]-DBP has six *cis*-butadiene conjugations and five *trans*-butadiene conjugations. After the subtraction, we obtain that all three species are, actually, stabilized by cyclic π-electron delocalization with the following energies: [*a*,*e*]-DBP 74.4 kcal/mol, closed-shell [*a*,*f*]-DBP 62.5 and open-shell singlet [*a*,*f*]-DBP 89.6 kcal/mol. Exclusion of the conjugation over the central CC bond (fusion of two pentagones) which is not involved in any cyclic delocalization and which is of similar strength in all species, 29.8-33.6 kcal/mol, lowers the energies to 44.6 kcal/mol, 29.0 kcal/mol and 56.3 kcal/mol, but does not change the obtained trend. Thus, according to the presented results, the less stable open-shell singlet [*a*,*f*]-DBP gains more stabilizing energy from cyclic π-electron delocalization than the more stable [*a*,*e*]-DBP (not the case for closed-shell [*a*,*f*]-DBP).

View Article Online
DOI: 10.1039/C8CP07875K

3.2.2. Estimation of electron delocalization on the basis of HOMA and FLU_π

Calculated delocalization indices, HOMA and FLU_π, support conclusions from energetic analysis and also allow us to identify a degree of electron delocalization of various circuits in the molecules. The values are given in Figure 3. They show that all subunits (five-membered rings, indene, pentalene, tricycles and molecular perimeter) of open-shell singlet [*a*,*f*]-DBP are more delocalized than the corresponding parts of [*a*,*e*]-isomer. The only exception are two benzene rings: one is less delocalized in open-shell singlet [*a*,*f*]-DBP and the other is weakly delocalized (HOMA = 0.405).

A slight increase in electron delocalization is observed for some substructures of closed-shell [*a*,*f*]-DBP relative to [*a*,*e*]-DBP (five-membered rings, indene which includes aromatic benzene ring and tricycle which includes aromatic benzene ring), while indene which comprises benzene with *ortho*-quinoidal structure, tricycle which comprises benzene with *ortho*-quinoidal structure and molecular perimeter are somewhat more delocalized according to HOMA, but slightly less so according to FLU_π. Hence, the main reason for the observed overall lower energetic stabilization due to cyclic π-electron delocalization of closed-shell [*a*,*f*]-DBP vs [*a*,*e*]-DBP can be attributed to the loss of aromaticity of one benzene ring in [*a*,*f*]-isomer, while another becomes only less aromatic. According to the calculated indices, the most delocalized parts of [*a*,*e*]-isomer are two benzene rings, and only one benzene in [*a*,*f*]-isomer (Figure 3E).

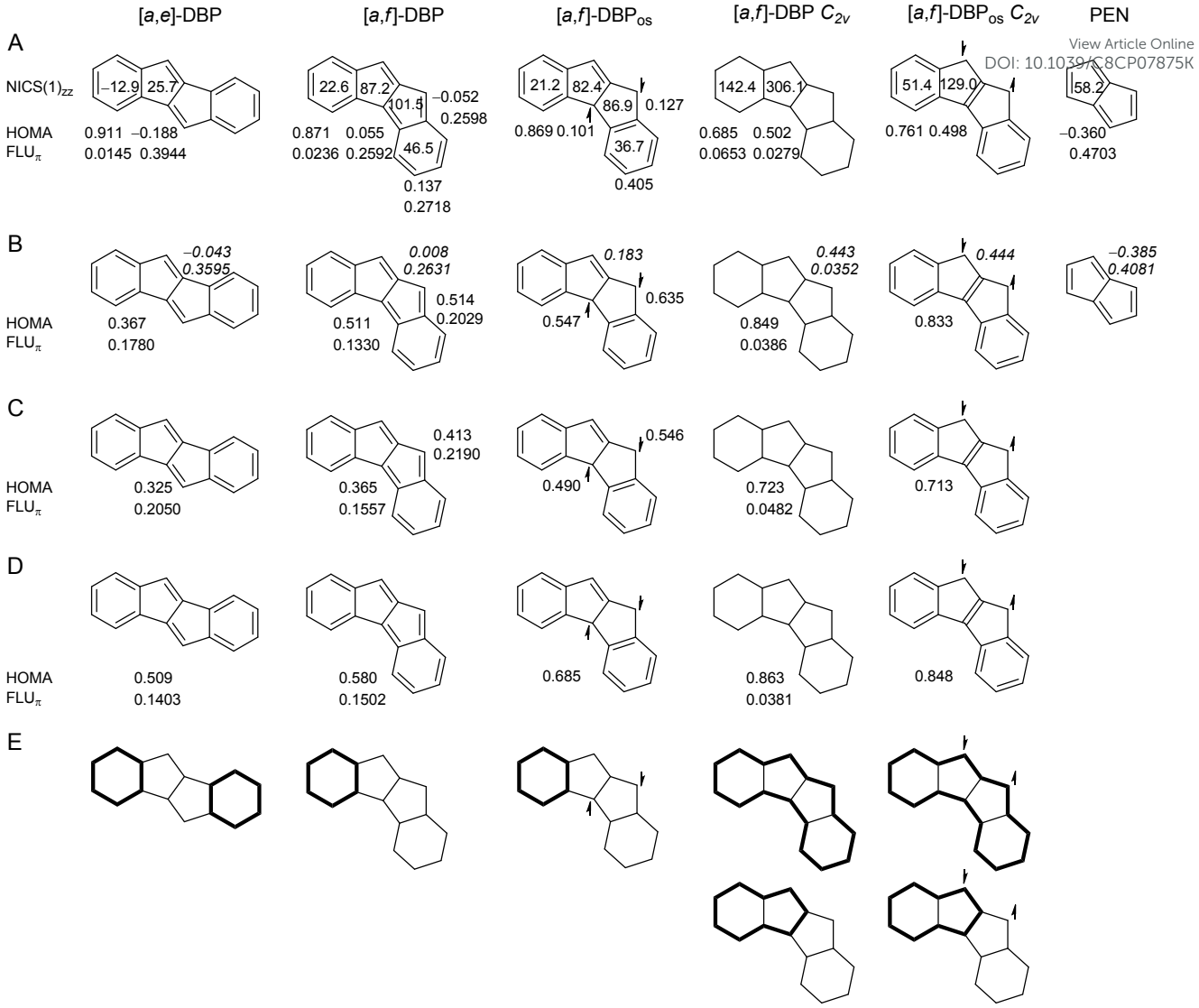

Figure 3. Calculated NICS(1)$_{zz}$, HOMA and FLU$_\pi$ for monocycles (A), HOMA and FLU$_\pi$ for bicycles, values in italic are for pentalene subunit (B), tricycles (C) and molecular perimeter (D) of dibenzopentalenes. The most delocalized (sub)units are shown in (E).

3.2.3. Energy decomposition analysis

After reaching at conclusion that the closed-shell/open-shell singlet [*a*,*f*]-DBP is similarly/more π-electron delocalized than the more stable [*a*,*e*]-DBP, and that all three species are more stabilized by cyclic π-electron delocalization compared to the acyclic reference, a question arises: what factors are responsible for energetic destabilization of [*a*,*f*]-DBP?

View Article Online
DOI: 10.1039/C8CP07875K

3.2.3.1. Closed-shell state of dibenzopentalenes

To answer the question we consider that [*a*,*f*]-DBP can be formed from [*a*,*e*]-DBP by the out-of-plane rotation of the 2-methylphenyltriyl triradical fragment (Figure 4A, the fragment is shown in bold). This isomerization process, proceeding with increase in energy by ΔE_{iso} = 21.67 kcal/mol (energy difference between [*a*,*f*]-DBP and [*a*,*e*]-DBP), involves breaking and formation of two bonds (shown in red in Figure 4A). Further electronic state change to open-shell singlet lowers the energy by ΔE_{es} = –0.32 kcal/mol.

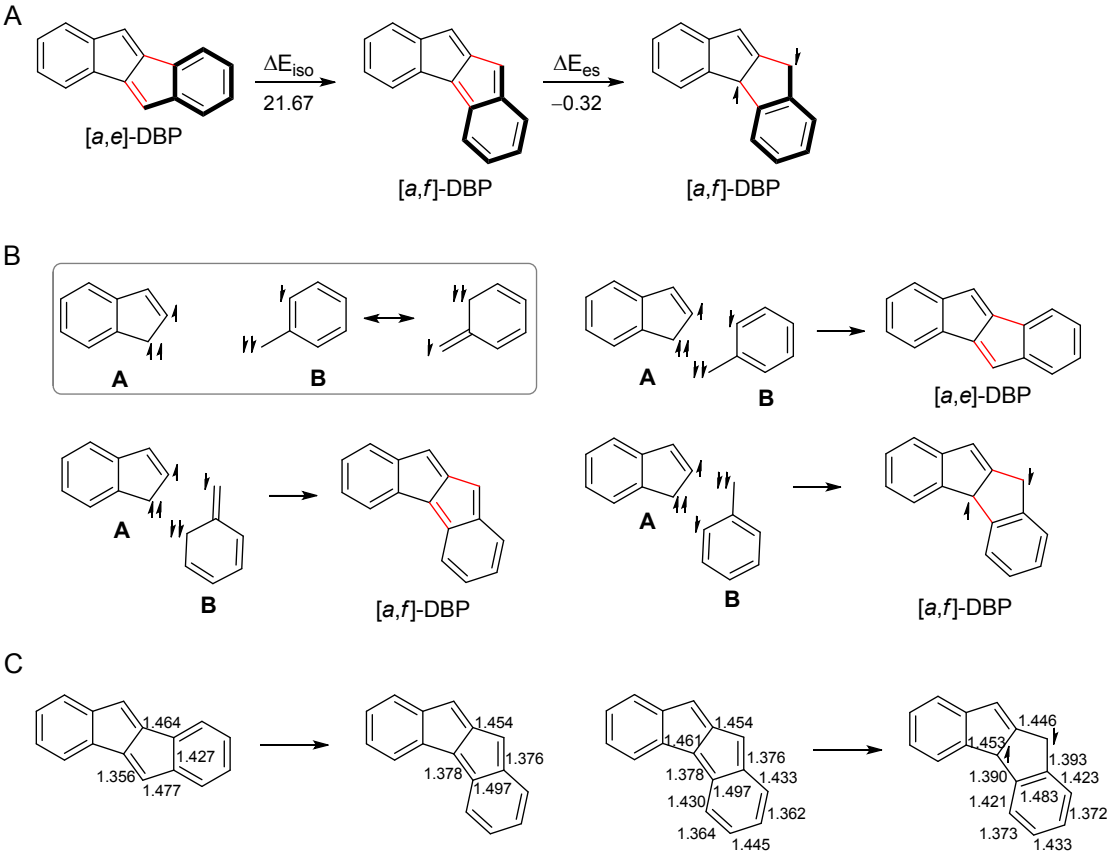

Figure 4. Isomerization of [*a*,*e*]-DBP into [*a*,*f*]-DBP and further formation of open-shell singlet [*a*,*f*]-DBP (A). Formation of [*a*,*e*]-DBP, [*a*,*f*]-DBP and [*a*,*f*]-DBP_{os} from fragments **A** and **B** (B). Most important structural changes during the isomerization and formation of open-shell [*a*,*f*]-DBP. Bond lengths are in Å (C).

In other words, if we start from two triradical fragments, **A** and **B**, we can form all three DBP species: [*a*,*e*]-DBP, [*a*,*f*]-DBP and open-shell singlet [*a*,*f*]-DBP (Figure 4B). For bonds fomation, the radical fragments should have opposite spin electrons. For closed-shell species two σ bonds and one π bond are formed, whereas for the open-shell singlet [*a*,*f*]-isomer two σ bonds are

View Article Online
DOI: 10.1039/C8CP07875K

formed and two electrons remain unpaired. Before **A** and **B** fragments form a compound, they have to deform to the geometry that they have in the final molecules. The required energy is deformation energy, ΔE_{def}. After the formation of chemical bonds from deformed fragments a certain amount of energy is released. It is interaction energy, ΔE_{int}. These two energies form the main parts of the total energy change, $\Delta E_{tot} = \Delta E_{def} + \Delta E_{int}$, occuring during the process: **A** + **B** $\rightarrow$ DBP. The interaction energy involves several types of interactions: classical electrostatic interactions, quantum-mechanical orbital interactions and dispersion. Electrostatic interactions (ΔE_{elstat}) can be attractive (electron-nucleus) and repulsive (electron-electron and nucleus-nucleus). Attractive interactions usually outweigh the repulsive ones, so that the total electrostatic energy is stabilizing. Quantum-mechanical orbital interactions can be repulsive (ΔE_{Pauli}, Pauli repulsion which is a consequence of the Pauli exclusion principle) and stabilizing (ΔE_{oi}, which involves bond formation from two opposite spin electrons, donor-acceptor interactions between occupied orbitals of one fragment and empty orbitals of another, and polarization, that is, the empty-occupied orbital mixing within one fragment due to the presence of another). Dispersion energy (ΔE_{disp}) is stabilizing. Dissection of ΔE_{int} into the above mentioned energy components was done by using the LMOEDA.[22,33] Therefore, the total energy change upon molecule formation from fragments **A** and **B** can be represented as in Eq. 1.

$$\Delta E_{tot} = \Delta E_{def} + \Delta E_{elstat} + \Delta E_{Pauli} + \Delta E_{oi} + \Delta E_{disp} \quad (1)$$

where the latter four components constitute the interaction energy (ΔE_{int}). Energy components for isomerization (ΔE_{iso}) and electronic state change processes (ΔE_{es}) are obtained as given in Eq. 2 and 3. Both the total energies, energy changes and their components are presented in Table 1.

$$[a,e]\text{-DBP} \xrightarrow{\Delta E_{iso}} [a,f]\text{-DBP} \xrightarrow{\Delta E_{es}} [a,f]\text{-DBP}_{os}$$

$$\Delta E_{iso} = \Delta E_{tot}([a,f]\text{-DBP}) - \Delta E_{tot}([a,e]\text{-DBP}) \quad (2)$$

$$\Delta E_{es} = \Delta E_{tot}([a,f]\text{-DBP}_{os}) - \Delta E_{tot}([a,f]\text{-DBP}) \quad (3)$$

View Article Online
DOI: 10.1039/C8CP07875K

As the first step of the discussion, we wish to point out what are the most important structural changes that accompany [*a*,*e*]-DBP → [*a*,*f*]-DBP isomerization (Figure 4C). Isomerization is followed by the double bond elongation by 0.022 Å and compression of the single bond by 0.01 Å. These two changes affect ΔE_{int}. The exocyclic bond of 2-methylphenyltriyl fragment shortens by 0.101 Å and the bond of the benzene ring at the fusion site increases its length by 0.07 Å. Other bonds in benzene ring elongate/shorten by 0.05/0.04 Å (not shown in the figure). Energy needed for these changes is included in ΔE_{def}. The largest bond angle changes are ~2° and are not shown in the Figure.

The values in Table 1 show that the main part of energy increase when going from [*a*,*e*]-DBP to [*a*,*f*]-DBP (entries 1, 2 and 10) comes from ΔE_{int} (94%), while ΔE_{def} contributes only 6%. Since the latter mostly involves structural changes due to benzene → *ortho*-quinoidal form transition, it can be concluded that this structural change constitute minor part of higher energy of [*a*,*f*]-isomer. Much more important are changes in bonding nature, where weakening in orbital interactions takes up the major part (75%) of less favourable ΔE_{int}. The decrease in electrostatic stabilization is responsible for 20% of weaker interaction energy and the decrease of dispersion stabilization for only 5%. The contribution from the latter is canceled by the weaker Pauli repulsion in [*a*,*f*]-DBP.

Table 1. Contribution of various energy components to the total binding interactions between fragments **A** and **B** (Figure 4) in dibenzopentalenes and energy changes (values in bold) upon constitutional isomerization, change in electronic state, or formation of transition state for C_s [*a*,*f*]-DBP structure equilibrations.[a] Values are in kcal/mol, calculated at the UB3LYP/6-311+G(d,p) level.

Entry	Molecule	ΔE_{tot} **ΔE**	ΔE_{def} **$\Delta\Delta E_{def}$**	ΔE_{int} **$\Delta\Delta E_{int}$**	ΔE_{elstat} **$\Delta\Delta E_{elstat}$**	ΔE_{Pauli} **$\Delta\Delta E_{Pauli}$**	ΔE_{oi} **$\Delta\Delta E_{oi}$**	ΔE_{disp} **$\Delta\Delta E_{disp}$**	Interacting fragments
1	[*a*,*e*]-DBP	-259.97	11.65	-271.62	-331.97	541.29	-421.31	-59.63	**A**(q)+**B**(q)
2	[*a*,*f*]-DBP	-238.30	12.99	-251.19	-327.53	539.53	-404.68	-58.61	**A**(q)+**B**(q)
3	[*a*,*f*]-DBP	-226.69	11.65	-238.45	-333.82	552.57	-397.37	-59.83	$\mathbf{A}^{a,e}$(q)+$\mathbf{B}^{a,e}$(q)
4	[*a*,*f*]-DBP	-237.69	13.41	-251.10	-333.11	552.13	-411.01	-59.11	$\mathbf{A}^{a,e}$(q)+$\mathbf{B}^{a,f}$(q)
5	[*a*,*f*]-DBP_{os}	-238.62	11.24	-249.86	-325.80	535.29	-401.96	-57.39	**A**(q)+**B**(q)
6	[*a*,*f*]-DBP C_{2v} TS	-235.77	14.10	-249.87	-322.48	527.28	-396.73	-57.94	**A**(q)+**B**(q)
7	[*a*,*f*]-DBP_{os} C_{2v} TS	-236.82	12.32	-249.14	-320.42	523.34	-395.17	-56.89	**A**(q)+**B**(q)
8	[*a*,*e*]-DBP T_1	-227.76	91.27	-319.03	-331.28	537.99	-461.88	-63.86	**A**(sext)+**B**(q)
9	[*a*,*f*]-DBP T_1	-238.52	91.84	-330.36	-322.52	518.74	-464.20	-62.38	**A**(sext)+**B**(q)
10	**[*a*,*e*] → [*a*,*f*]**	**21.67**	**1.34**	**20.33**	**4.44**	**-1.76**	**16.63**	**1.02**	
11	**[*a*,*e*] → [*a*,*f*]**$^{\mathbf{A}a,e+\mathbf{B}a,e}$	**33.17**	**0.00**	**33.17**	**-1.85**	**11.28**	**23.94**	**-0.20**	
12	**[*a*,*f*]**$^{\mathbf{A}a,e+\mathbf{B}a,e}$ **→ [*a*,*f*]**$^{\mathbf{A}a,e+\mathbf{B}a,f}$	**-11.00**	**1.65**	**-12.65**	**0.71**	**-0.44**	**-13.64**	**0.72**	
13	**[*a*,*f*]**$^{\mathbf{A}a,e+\mathbf{B}a,f}$ **→ [*a*,*f*]**	**-0.61**	**-0.42**	**-0.19**	**5.58**	**-12.60**	**6.33**	**0.50**	
14	**[*a*,*f*] → [*a*,*f*]**$_{os}$	**-0.32**	**-1.75**	**1.43**	**1.73**	**-4.24**	**2.72**	**1.22**	
15	**[*a*,*e*] → [*a*,*f*]$_{os}$**	**21.35**	**-0.41**	**21.76**	**6.17**	**-6.00**	**19.35**	**2.24**	
16	**[*a*,*f*] → [*a*,*f*]** C_{2v}	**2.53**	**1.11**	**1.42**	**5.05**	**-12.25**	**7.95**	**0.67**	
17	**[*a*,*f*]**$_{os}$ **→ [*a*,*f*]**$_{os}$ C_{2v}	**1.79**	**1.07**	**0.72**	**5.38**	**-11.95**	**6.79**	**0.50**	
18	**[*a*,*e*]** T_1 **→ [*a*,*f*]** T_1	**-10.76**	**0.57**	**-11.33**	**8.76**	**-19.25**	**-2.32**	**1.48**	
19	**[*a*,*e*] → [*a*,*e*]** T_1	**32.22**	**79.63**	**-47.41**	**0.69**	**-3.03**	**-40.57**	**-4.23**	
20	**[*a*,*f*] → [*a*,*f*]** T_1	**-0.22**	**78.85**	**-79.07**	**5.01**	**-20.79**	**-59.52**	**-3.77**	
21	**[*a*,*f*]**$_{os}$ **→ [*a*,*f*]** T_1	**0.10**	**80.60**	**-80.50**	**3.28**	**-16.55**	**-62.24**	**-4.99**	

[a] ΔE_{tot} = total binding energy between two fragments, ΔE_{def} = deformation energy, ΔE_{int} = interaction energy, ΔE_{elstat} = electrostatic energy, ΔE_{Pauli} = Pauli repulsion, ΔE_{oi} = orbital interaction energy, ΔE_{disp} = dispersion energy, ΔE = energy change upon isomerization, electronic state change, or formation of transition state.

A decrease in the breaking/forming single bond length upon isomerization (0.01 Å, Figure 4C) streghtens the electron pair bonding, while π-electron delocalization over that bond is rather similar in the two isomers, which is evident from the already discussed π-electron delocalization energy (which is comparable for the two isomers), HOMA and FLU_π data in Figure 3 and delocalization energy of the *cis*-butadiene/*trans*-butadiene subunits in [*a*,*e*]/[*a*,*f*]-isomers, which are 28.3 kcal/mol and 32.1 kcal/mol, respectively. Thus, it is the weakening of σ and π components of

View Article Online
DOI: 10.1039/C8CP07875K

the breaking/forming double bond which is responsible for the decrease in orbital interaction energy of [*a*,*f*]-DBP. This bond elongation also leads to decrease in electrostatic stabilization, which is another factor involved in the weaker bonding of [*a*,*f*]-DBP.

However, an analysis of only equilibrium geometry of higher energy [*a*,*f*]-DBP may hide some important facts. For this reason, we also performed the following analysis. The [*a*,*f*]-DBP was formed from exactly the same fragments of which [*a*,*e*]-isomer is composed ($\mathbf{A}^{a,e}$ and $\mathbf{B}^{a,e}$). This means that fragment **B** was simply out-of-plane rotated without any changes in geometry. The two interconnecting bonds were also kept with the same length which they had in [*a*,*e*]-DBP. The associated ΔE_{iso} = 33.17 kcal/mol (Figure 5) reflects solely the change in the bonding nature, while deformation energy vanishes. Next we explored the energy change (ΔE_{bl}) when interconnecting bonds were shortened/elongated to the distances of the optimized [*a*,*f*]-DBP (red colour in the figure) while still keeping the two fragments in their [*a*,*e*]-geometry and the energy change (ΔE_{struct}) when fragment $\mathbf{B}^{a,e}$ relaxes into its [*a*,*f*]-geometry $\mathbf{B}^{a,f}$ (blue colour in the figure) while the interconnecting bonds remained frozen. Whereas the change of bond lengths had a slight stabilizing effect $\Delta E_{bl} = -1.10$ kcal/mol, the structural relaxation of fragment **B** decreased the energy by $\Delta E_{struct} = -10.97$ kcal/mol. The same structural change starting from [*a*,*f*]-DBP composed of $\mathbf{A}^{a,e}$ and $\mathbf{B}^{a,e}$ fragments and having its equilibrium lengths of interconnecting bonds stabilized the system by $\Delta E_{struct} = -10.05$ kcal/mol (Figure 5), while the bond lenghts change of [*a*,*f*]-DBP consisting of $\mathbf{A}^{a,e}$ and $\mathbf{B}^{a,f}$ reduced the energy by only $\Delta E_{bl} = -0.18$ kcal/mol. In both cases the [*a*,*f*]-DBP having just the **A** fragment with [*a*,*e*]-geometry was obtained. Further structural relaxation of this fragment, $\mathbf{A}^{a,e} \rightarrow \mathbf{A}^{a,f}$, to give the optimized [*a*,*f*]-DBP had just a slight stabilizing effect, $\Delta E_{struct} = -0.35$ kcal/mol. This analysis reveals the hidden fact that the final geometry of [*a*,*f*]-DBP, suffering from weaker orbital and electrostatic stabilization, is driven by the structural change of PhCH subunit. Next question that has to be answered is which factors are responsible for this change.

View Article Online
DOI: 10.1039/C8CP07875K

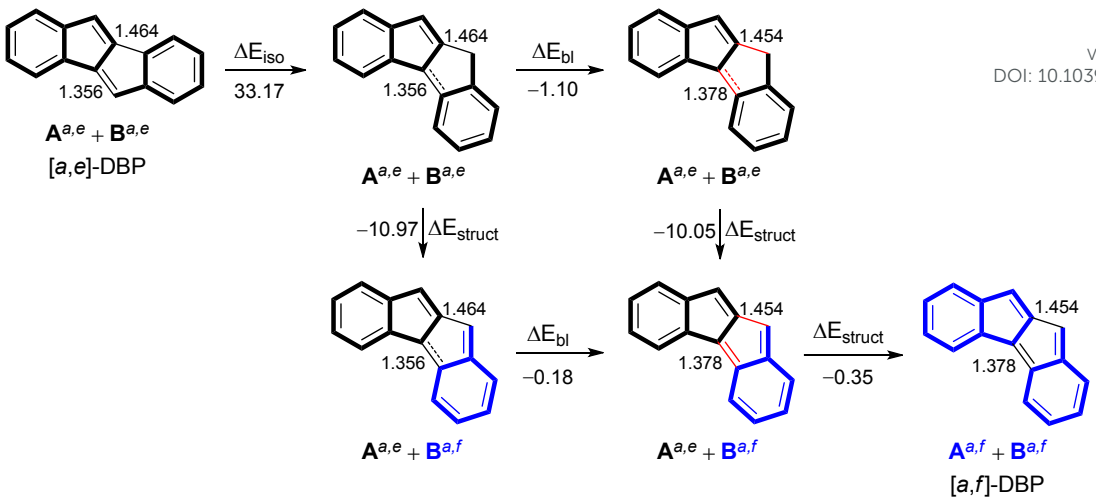

Figure 5. Energy change associated with simple [*a*,*e*]-DBP → [*a*,*f*]-DBP isomerization without any change in geometry and the effects of fragment **B** structural relaxation, interconnecting bond length changes and fragment **A** structural relaxation on molecular energy.

Since $\mathbf{B}^{a,e} \rightarrow \mathbf{B}^{a,f}$ structural change is the most important energy releasing factor, we examined the energy decomposition data and aromaticity indices changes for the following processes: [*a*,*e*]-DBP$^{\mathbf{A}a,e+\mathbf{B}a,e}$ → [*a*,*f*]-DBP$^{\mathbf{A}a,e+\mathbf{B}a,e}$ (frozen interconnecting bonds) → [*a*,*f*]-DBP$^{\mathbf{A}a,e+\mathbf{B}a,f}$ (frozen interconnecting bonds) → [*a*,*f*]-DBP$^{\mathbf{A}a,f+\mathbf{B}a,f}$ (equilibrium interconnecting bonds). The last process invloves interconnecting bond lengths changes and structural relaxation of fragment **A**. The EDA data are listed in Table 1 (entries 1-4 and 11-13) and aromaticity indices are shown in Table 2. Thus, the pure formation of [*a*,*f*] topology does not change HOMA data because all bonds retain their lengths (Table 2, entries 5 and 6), but affects the π-electron delocalization which increases in all subunits and at molecular perimeter, except for benzene rings which become less delocalized, (FLU_π data in Table 2, entries 9 and 10). Although, our traditional chemical knowledge tells us that the more delocalized system should be more stable, this is not necessarily true. The EDA results show that the increased π-electron delocalization significantly reduces the orbital interaction energy, $\Delta\Delta E_{oi}$ = 23.94 kcal/mol, which accounts for ~2/3 of energy rise when going from [*a*,*e*] to [*a*,*f*] topology (Table 1, entry 11). In fact, the more delocalized π-system the weaker is the π-bonding within the chemical bond.[34] In addition, the [*a*,*f*] topology suffers from

View Article Online
DOI: 10.1039/C8CP07875K

increased Pauli destabilization, accouning for ~1/3 of total energy rise, and creates an enormous global paratropicity involving all four monocyclic subunits (Table 2, entry 2). The subsequent PhCH substructure relaxation increases BLA in cyclopentadiene ring, benzene ring and central pentalene moiety (HOMA data in Table 2, entries 6 and 7) and decreases π-electron delocalization at molecular perimeter and in all subunits except benzene of fragment **A**, which slightly enhances its delocalization (Table 2, entries 10 and 11). This change considerably reduces paratropicity (Table 2, entry 3). The EDA data show that this increased localization of the π-electronic system significantly streghtens orbital interaction energy component $\Delta\Delta E_{oi} = -13.64$ kcal/mol (Table 1, entry 12), which is the major cause (97%) for decrease in energy. The final step, involving interconnecting bond changes to their equilibrium lengths in [*a*,*f*]-DBP and fragment **A** structural change, results in the large decrease in the Pauli repulsion $\Delta\Delta E_{Pauli} = -12.60$ kcal/mol which is counteracted by the decrease in electrostatic and orbital stabilization, $\Delta\Delta E_{elstat} = 5.58$ kcal/mol and $\Delta\Delta E_{oi} = 6.33$ kcal/mol, so that the total energy change, benefiting also from $\Delta\Delta E_{def} = -0.42$ kcal/mol, is small (Table 1, entry 13).

Table 2. Calculated NICS(1)$_{zz}$, HOMA and FLU$_{\pi}$ values for [*a*,*e*]-DBP, [*a*,*f*]-DBP having $\mathbf{A}^{a,e}$ and $\mathbf{B}^{a,e}$ fragments and interconnecting bonds as in [*a*,*e*]-DBP, [*a*,*f*]-DBP having $\mathbf{A}^{a,e}$ and $\mathbf{B}^{a,f}$ fragments and interconnecting bonds as in [*a*,*e*]-DBP and [*a*,*f*]-DBP.[a]

Entry			benz	cpd	cpd	benz	ind	ind	pent	tricycle	tricycle	peri
1	[*a*,*e*]	NICS(1)$_{zz}$	-12.9	25.7	25.7	-12.9						
2	$[a,f]^{\mathbf{A}a,e+\mathbf{B}a,e}$		182.2	376.7	493.9	275.5						
3	$[a,f]^{\mathbf{A}a,e+\mathbf{B}a,f}$		16.8	80.3	93.0	43.5						
4	[*a*,*f*]		22.7	87.2	101.5	46.5						
5	[*a*,*e*]	HOMA	0.911	-0.188	-0.188	0.911	0.367	0.367	-0.043	0.325	0.325	0.509
6	$[a,f]^{\mathbf{A}a,e+\mathbf{B}a,e}$		0.911	-0.188	-0.188	0.911	0.367	0.367	-0.042	0.325	0.325	0.509
7	$[a,f]^{\mathbf{A}a,e+\mathbf{B}a,f}$		0.911	-0.188	-0.320	0.137	0.367	0.366	-0.126	0.270	0.324	0.508
8	[*a*,*f*]		0.871	0.055	-0.052	0.137	0.511	0.514	0.008	0.365	0.413	0.580
9	[*a*,*e*]	FLU$_{\pi}$	0.0145	0.3944	0.3944	0.0145	0.1780	0.1780	0.3595	0.2050	0.2050	0.1403
10	$[a,f]^{\mathbf{A}a,e+\mathbf{B}a,e}$		0.0210	0.2420	0.1540	0.1266	0.1258	0.1047	0.1940	0.1233	0.1358	0.0954
11	$[a,f]^{\mathbf{A}a,e+\mathbf{B}a,f}$		0.0192	0.3208	0.3004	0.2907	0.1544	0.2246	0.2967	0.1729	0.2396	0.1645
12	[*a*,*f*]		0.0236	0.2592	0.2598	0.2718	0.1330	0.2029	0.2631	0.1557	0.2190	0.1502

[a] Abbreviations: benz (benzene), cpd (cyclopentadiene), ind (indene), pent (pentalene), peri (molecular perimeter).

Briefly, it is the π-electronic system which is mainly responsible for the energy difference between the two DBP isomers. Thus, the [*a*,*f*] topology features rather delocalized π-system, which significantly weakens its π-bonding energy, the streghtening of which acts as a driving force for PhCH substructure deformation leading to a substantial decrease in energy (ΔE = −10.97 kcal/mol). The final geometry, which is just slightly lower in energy (ΔE = −0.53 kcal/mol), is obtained by the additional Pauli repulsion relief on account of a decrease in orbital and electrostatic stabilization. Thus, as mentioned above, this final [*a*,*f*]-DBP structure suffers mostly from weaker orbital interactions and less from weaker electrostatic energy.

3.2.3.2. Closed-shell/open-shell singlet transition of [*a*,*f*]-DBP

A transition from electron-paired singlet into an open-shell singlet state of [*a*,*f*]-DBP lowers the energy slightly, $\Delta E_{es} = -0.32$ kcal/mol. To trace the factors responsible for experimentally and computationally proven tendency of [*a*,*f*]-isomer to attain the open-shell structure we explore the energy decomposition data from Table 1, entries 2, 5 and 14). While interaction energy drops (become less stabilizing) by $\Delta\Delta E_{int} = 1.43$ kcal/mol, structural changes, involved in the deformation energy, $\Delta\Delta E_{def} = -1.75$ kcal/mol, lead to the slightly more stable structure. The most important structural changes are given in Figure 4C and majority of them are associated with the electronic rearrangement to the 6π-electron benzene subunit. Hence, the regaining of aromaticity of benzene can be considered as the driving force toward the diradical state of [*a*,*f*]-isomer, which occurs on account of a slight loss of orbital ($\Delta\Delta E_{oi} = 2.72$ kcal/mol), electrostatic ($\Delta\Delta E_{elstat} = 1.73$ kcal/mol) and dispersion interactions ($\Delta\Delta E_{disp} = 1.22$ kcal/mol), but a drop in the Pauli repulsion ($\Delta\Delta E_{Pauli} = -4.24$ kcal/mol). Since closed-shell → open-shell singlet transition of [*a*,*f*]-isomer mainly involves changes of *ortho*-quinodimethane subunit, we also performed a slightly different energy decomposition analysis in which focus was on the two exocyclic bonds of the mentioned subunit. Details are given in the ESI (Section S1) and the results led to the same conclusion that the process is driven by the formation of Hückel aromatic benzene subunit. In other words, the closed-shell [*a*,*f*]-DBP contains pro-aromatic subunit, the transition of which to the 6π-electron one leads to open-shell singlet state. Polycyclic compounds comprising pro-aromatic substructures often show a tendency to exist as diradicals.[35]

Now, comparing the most stable open-shell state of [*a*,*f*]-DBP and the lower energy [*a*,*e*]-isomer the former is destabilized only by the weaker bonding, $\Delta E_{int} = 21.76$ kcal/mol (Table 1, entries 1, 5 and 15). This mainly comes from weaker orbital interactions (σ and π). The π-component is weaker because of the larger π-electron delocalization, while σ-component weakening results from the 0.034 Å doble bond elongation (Figure 4C). The minor part of energy

difference originates from smaller dispersion stabilization, while $\Delta\Delta E_{elstat}$ and $\Delta\Delta E_{Pauli}$ mostly cancel each other.

View Article Online
DOI: 10.1039/C8CP07875K

3.2.3.3. Energy barrier for interconversion of C_s structures of [*a*,*f*]-DBP

According to our calculations, the two C_s singlet structures of [*a*,*f*]-DBP need small energy of 2.53 kcal/mol (closed-shell) and 1.79 kcal/mol (open-shell) to equilibrate. The EDA results from Table 1 (entries 2, 5-7, 16 and 17) indicate that deformation energy is the significant cause for this barrier (44% for closed-shell system and 63% for open-shell system). Examination of optimized structures reveals that formation of C_{2v} structures needs all bonds to be elongated or shortened by 0.02-0.06 Å for closed-shell system and 0.01-0.04 Å for open-shell system. Bond angle changes are less pronounced. These TS C_{2v} structures are characterized by decreased BLA and the associated increased π-electron delocalization of all subunits and molecular perimeter, except one benzene (HOMA and FLU_π data in Figure 3). The largest delocalization shifts from one benzene in the GS structures to the molecular perimeter and perimeter of indene subunits in TS structures (Figure 3E). This significantly enhances paratropicity of closed-shell species ($NICS(1)_{zz}$ = 142.4 ppm and 306.1 ppm for benzene and cyclopentadiene moieties, respectively) and less so of the open-shell one ($NICS(1)_{zz}$ = 51.5 ppm and 129.0 ppm). The increased π-electron delocalization is partly reflected in weaker orbital interactions in TS structures, $\Delta\Delta E_{oi}$ = 7.95 kcal/mol and 6.79 kcal/mol for closed-shell and open-shell systems, respectively, another part coming from a decrease in σ bond strength due to 0.04-0.05 Å elongation of the bond connecting the **A** and **B** fragments. Another important factor for the energy barrier is weakening of electrostatic stabilization ($\Delta\Delta E_{elstat}$ = 5.05 kcal/mol and 5.38 kcal/mol for closed-shell and open-shell systems, respectively), while repulsion energy significantly decreases, $\Delta\Delta E_{Pauli}$ = −12.25 kcal/mol and −11.95 kcal/mol. Since the C_{2v} structures are very close in energy to C_s structures, it is highly probable that some derivatives of [*a*,*f*]-DBP adopt such symmetrical structures with increased paratropicity.

View Article Online
DOI: 10.1039/C8CP07875K

3.3. Triplet states of dibenzopentalenes

According to the Baird's rule,[36] there is an antiaromaticity/aromaticity switch when going to the first excited triplet state. This means that antiaromatic compounds become aromatic in their triplet state and vice versa. The triplet state of [*a*,*e*]-DBP was examined before and was shown to sustain diatropic currents throughout the whole molecule, with slight enhancement in the five-membered rings.[12] Our calculated $NICS(1)_{zz}$ values, shown in Figure 6, agree with the overall diatropicity of [*a*,*e*]-DBP ($NICS(1)_{zz}$ = −23.6 ppm and −32.9 ppm for benzene and cyclopentadiene rings, respectively), as well as the NICS-*XY* scans discussed in Section 3.4. The HOMA values show a slight increase/decrease in BLA of six- and five-membered subunits, relative to the singlet ground state (compare data in Figures 3 and 6). According to HOMA, the most delocalized circuit in the molecule is its perimeter (Figure 6D).

Another isomer of DBP has not been studied in its triplet state, which is very close in energy to the open-shell singlet (0.1 kcal/mol, Figure 2) and can be easily reached by thermal excitation.[16] The HOMA data show a decrease in BLA of all subunits and molecular perimeter of triplet [*a*,*f*]-DBP, compared to its singlet states, except one benzene ring which has slightly increased BLA (compare Figures 3 and 6). According to the same index, the most delocalized parts of triplet [*a*,*f*]-DBP are the two benzene rings (Figure 6D). The NICS data indicate a large change in magnetic properties upon singlet/triplet excitation: the paratropicity of six- and five-membered rings turns into diatropicity, which is more pronounced in benzene than in cyclopentadiene rings (Figure 6A). Compared to the triplet [*a*,*e*]-isomer, benzene ring of [*a*,*f*] is slightly more aromatic, while cyclopentadiene is much less diatropic.

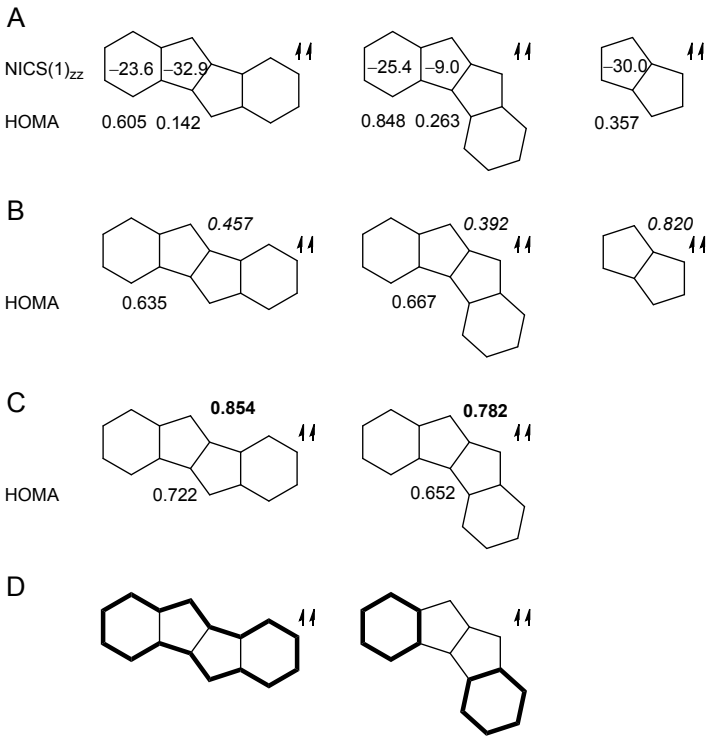

Figure 6. Calculated NICS(1)$_{zz}$ and HOMA for monocycles (A), bicycles, values in italic are for pentalene subunit (B), tricycles and molecular perimeter (bolded) of dibenzopentalenes (C). The most delocalized (sub)units are shown in (D).

3.3.1. Energy decomposition analysis

While singlet state of [*a*,*f*]-DBP is by 21.67 kcal/mol (closed-shell) and 21.35 kcal/mol (open-shell) less stable than [*a*,*e*]-DBP, there is a reversal of stability of the two isomers in their triplet states where [*a*,*f*]-DBP is more stable by 10.76 kcal/mol. To search for the origin of this effect we performed the isomerization EDA in which the same interacting fragments **A** and **B** were taken in their sextet and quartet electronic states, respectively (Figure 7A). The isomerization process was carried out as before, by the out-of-plane rotation of fragment **B**. The bond lengths, and their change, are consistent with the spin density distribution over the pentalene moiety in [*a*,*e*]-DBP, but over the trimethylenemethane subunit in [*a*,*f*]-DBP (Figure 7B). Bond angle changes are small, $< 1.5°$, and are not shown in the figure.

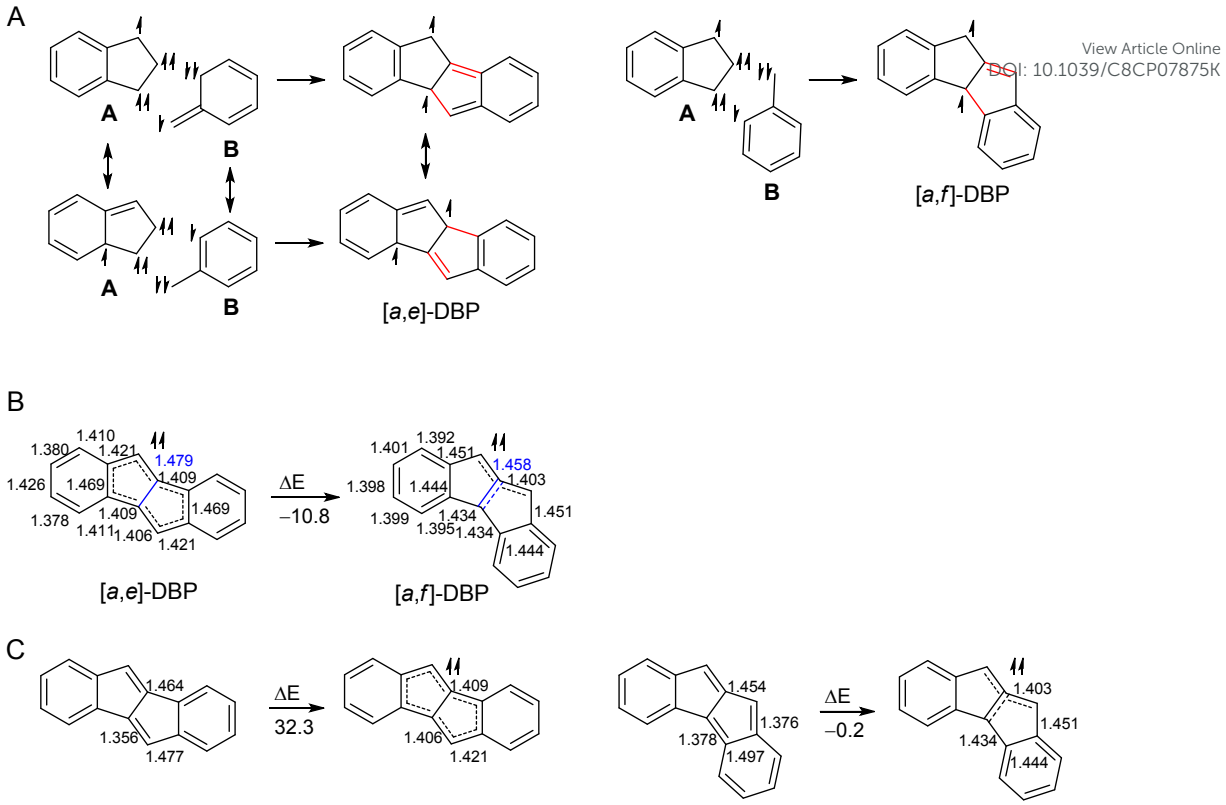

Figure 7. Formation of triplet states of [*a*,*e*]-DBP and [*a*,*f*]-DBP from fragments **A** and **B** (A). Most important structural changes occuring during the [*a*,*e*]-DBP → [*a*,*f*]-DBP isomerization in the triplet state (B). Most important structural changes that follow singlet/triplet excitation of [*a*,*e*]-DBP and [*a*,*f*]-DBP (C). Bond lengths are in Å, bond angles are in degrees.

The EDA results, given in Table 1 (entries 8, 9 and 18), show that deformation energy change is small, $\Delta\Delta E_{def} = 0.57$ kcal/mol, and is not the source of larger stability of triplet [*a*,*f*]-DBP (ΔE_{def} slightly favours [*a*,*e*] topology). The interaction energy terms reveal that orbital interactions are, now, slightly more favoured in [*a*,*f*]-DBP, $\Delta\Delta E_{oi} = -2.32$ kcal/mol, while electrostatic and dispersion interactions favour the [*a*,*e*] topology, $\Delta\Delta E_{elstat} = 8.76$ kcal/mol and $\Delta\Delta E_{disp} = 1.48$ kcal/mol. What is responsible for the main part (89%) of energy lowering upon triplet [*a*,*e*]-DBP → [*a*,*f*]-DBP isomerization is much smaller Pauli destabilization of the latter, $\Delta\Delta E_{Pauli} = -19.25$ kcal/mol. This can, partly, be explained by the ways in which the two topologies distribute the same spin electron density. Distribution over the central trimethylenemethane subunit in [*a*,*f*]-DBP separates the same spin electrons from benzene π-system, while their distribution over the central pentalene moiety results in larger repulsion.

DOI: 10.1039/C8CP07875K

Another difference between the [*a*,*e*]/[*a*,*f*]-DBP isomers is that the former needs 32.22 kcal/mol to reach the triplet state, while for the latter this process goes with molecular stabilization by 0.22 kcal/mol starting from the closed-shell singlet or needs only 0.1 kcal/mol starting from the open-shell singlet. The most important structural changes that follow the singlet/triplet transition are shown in Figure 7C. Bond angle changes do not exceed 2°. For both isomers the large $\Delta\Delta E_{def}$ of 79-80 kcal/mol (Table 1, entries 1, 2, 5, 8, 9 and 19-21) mostly reflects the energy needed to change the electronic state of the fragments. An increase in the strength of chemical bonding in [*a*,*f*]-DBP goes with the comparable energy change of 79-80 kcal/mol (entries 20 and 21), but with much less in [*a*,*e*]-DBP, $\Delta\Delta E_{int} = -47.41$ kcal/mol (entry 19). The reason for this is larger enhancement of orbital interactions in [*a*,*f*]-DBP upon going to triplet state and larger relief in Pauli repulsion (Table 1, entries 19-21). This can, again, be attributed to different unpaired spin distributions in the two isomers. Thus, in [*a*,*f*]-DBP there would be stronger π-bonding in the double bond marked in red in Figure 7B, but less so in [*a*,*e*]-DBP because of the resonance shown in the figure (the changes of the interconnecting bond lengths upon singlet/triplet transition are almost the same for both isomers, Figure 7C). The more favoured Pauli repulsion in the triplet [*a*,*f*]-DBP has already been discussed above.

3.4. NICS-*XY*-Scans: Evaluation of π-electron currents in pentalene and dibenzopentalenes

The π-electron currents in polycyclic compounds are determined by the nature of their substructures and are not easily predictive, particularly not in cases when elementary (sub)units contain 4*n*π- and (4*n*+2)π-electrons. Yet, they influence molecular properties and, thus, possible applications in organic electronics. While [*a*,*e*]-DBP was studied before,[12] it is of interest, here, to explore the nature of induced currents in the isomeric [*a*,*f*]-DBP and also how different topologies affect pentalene's (anti)aromaticity.

3.4.1. Singlet states

As noted at the beginning, pentalene is unstable, highly antiaromatic compound. It shows pronounced BLA in both cyclopentadienes and molecular perimeter, as evidenced by the HOMA data in Figure 3A and B). The FLU_{π} indicates little π-electron delocalization in monocycles and at molecular periphery, while $NICS(1)_{zz}$ shows large paratropicity, 58.2 ppm. The NICS-*XY*-scan, shown in Figure 8a, is consistent with the global paratropic currents and two smaller local paratropic currents in each ring. These data agree with the previously calculated NICS-*XY*-scan of the ground state of pentalene.[18f] Dibenzo-annulation in the [*a*,*e*] manner decreases the BLA of monocycles and molecular perimeter (HOMA data in Figure 3A and B), increases π-electron delocalization (FLU_{π} data in Figure 3A and B), and decreases paratropicity of cyclopentadiene rings ($NICS(1)_{zz}$ = 25.7 ppm). The NICS-*XY*-scan in Figure 8b shows that the formed [*a*,*e*]-DBP is characterized by two local diatropic ring currents in benzene rings (weaker than in benzene itself), weak global paratropic currents along the perimeter of pentalene subunit and two local paratropic currents in each five-membered ring. Hence, the topology and the type of ring currents in pentalene are retained upon dibenzoannulation, only their intensity is reduced.

Dibenzo-annulation in the [*a*,*f*] manner increases π-electron delocalization at molecular perimeter of pentalene and at each five-membered ring to greater extent than [*a*,*e*] topology does and the effect is more prominent in the open-shell singlet state (HOMA and FLU_{π} data in Figure 3A and B). Contrary to the [*a*,*e*] case, both local and global paratropicity of pentalene increases upon [*a*,*f*]-type fusion (Figures 3A, 8a and c). The NICS-*XY*-scan in Figure 8c is consistent with the global paratropic ring currents of [*a*,*f*]-DBP, possibly semi-global paratropic currents at the perimeter of pentalene subunit and two local paratropic currents in each five-membered ring, slightly more intense in the ring fused to benzene that lacks the π-electron sextet. Transition to the open-shell singlet state slightly reduces paratropicity at all levels, more so in one-half of the molecule carrying the unpared spin density, and this is also description given by the single NICS calculations from Figure 3A. The paratropicity of benzene rings in closed-shell and open-shell

View Article Online
DOI: 10.1039/C8CP07875K

singlet [*a*,*f*]-DBP (Figures 3A and 8c), also seen in current density maps of ref. 11a, can be interpreted as the net result of the local diatropic ring currents outweighed by the global paratropic currents of DBP. The superposition of these currents can be a cause of not much different NICS values of the two benzene rings in the closed-shell species, even though the HOMA and FLU_{π} data in Figure 3A indicate very different degree of aromaticity of these rings. Increase in symmetry of [*a*,*f*]-DBP drastically increases paratropicity at all levels, which is significantly decreased upon transition to the open-shell singlet state. However, the open-shell C_{2v} structure is still more paratropic than the lower symmetry ground states (Figure 3A and 8c).

Hence, while [*a*,*e*] topology retains, but weakens, induced currents of elementary subunits of DBP (benzene and pentalene), the [*a*,*f*] one creates an intense global paratropic currents which enhance total pentalene's paratropicity and involve benzene rings, as well.

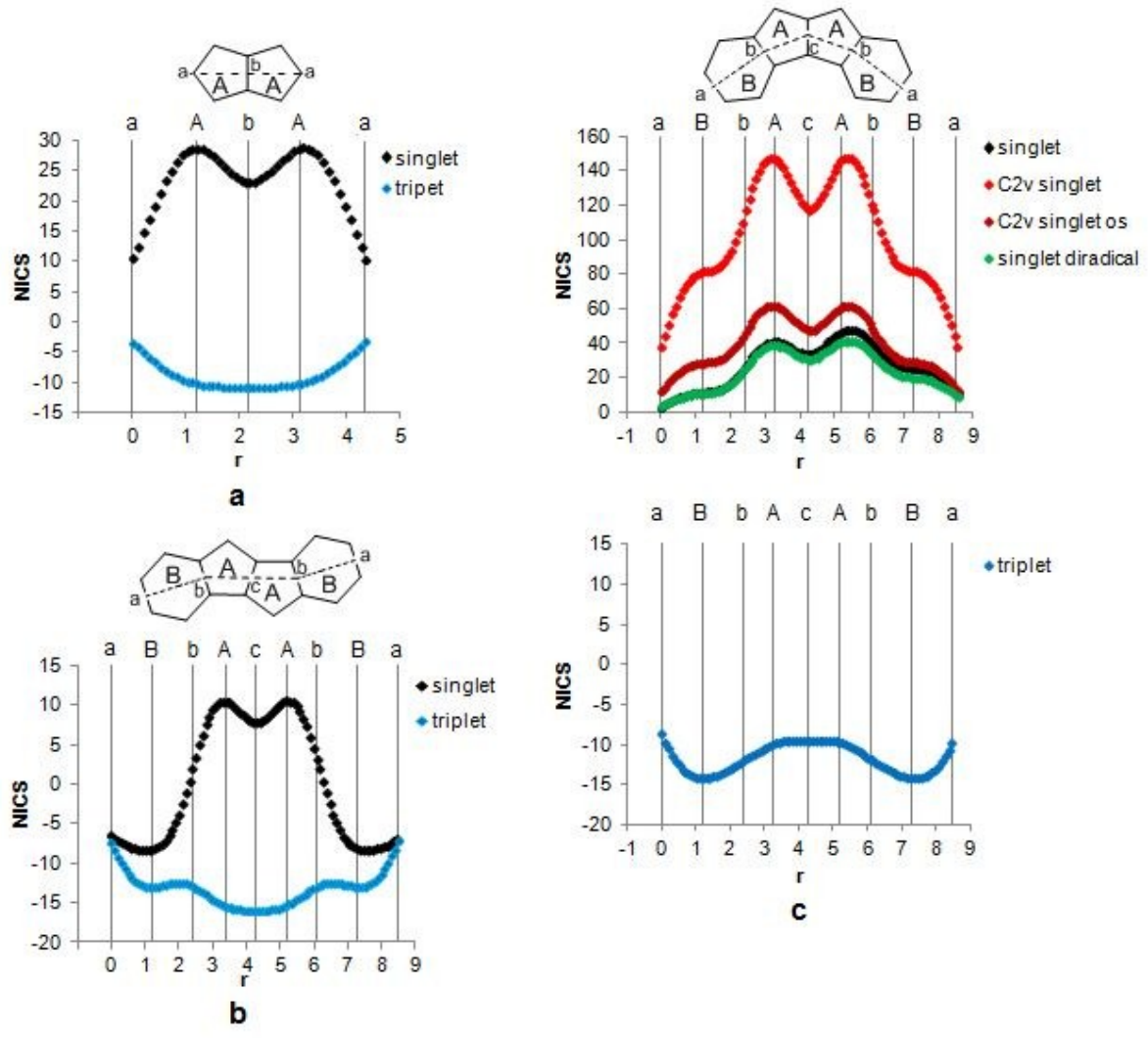

Figure 8. NICS-*XY*-scans of pentalene (a), [*a*,*e*]-dibenzopentalene (b) and [*a*,*f*]-dibenzopentalene (c) in their singlet and triplet states.

View Article Online
DOI: 10.1039/C8CP07875K

3.4.2. Triplet states

The triplet state of pentalene has significantly delocalized molecular perimeter and moderately delocalized cyclopentadiene rings (HOMA data in Figure 6A and B). The flat shape of the curve obtained by the NICS-*XY*-scan (Figure 8a) points to the global diatropic ring currents along molecular perimeter, with no local currents.

Both types of dibenzo-annulation significantly increase BLA of pentalene's perimeter and less so of its constituent monocycles (HOMA data in Figure 6). The NICS-*XY*-scans in Figures 8b and 8c are consistent with the global diatropicity of both [*a*,*e*]- and [*a*,*f*]-DBP, having also local diatropic currents at benzene rings, slightly more intense in the latter. The central parts of the curves, corresponding to pentalene subunit, are flat for both compounds, and represent a minimum for the former and maximum for the latter. For [*a*,*e*]-DBP, this can be interpreted as a superposition of global ring currents and semi-global pentalene's currents, which are weaker than in pentalene itself, since the NICS values in Figure 8b are just slightly more negative than in Figure 8a (~5 ppm). In the case of [*a*,*f*]-DBP, the flat maximum of the curve, along with the HOMA = 0.392 and $NICS(1)_{zz}$ = −9.0 ppm, suggest little aromaticity, if at all, of pentalene subunit. HOMA data and NICS-*XY*-scans indicate that the highest delocalization is at molecular periphery of [*a*,*e*]-DBP, but at benzene rings in [*a*,*f*]-DBP (Figure 6D). Thus, the existance of two Hückel aromatic benzene rings can also be seen as a source of low energy triplet state of [*a*,*f*]-DBP.

Therefore, it can be concuded that the two topologies of dibenzo-annulation of pentalene have opposite effects on its antiaromaticity in singlet state, but the same effect on its aromaticity in triplet state, where the [*a*,*f*] type attenuates it to greater extent. Recalling that singlet-triplet states should be easily interconvertible for the latter, pentalene moiety would behave as highly antiaromatic (singlet), or as almost nonaromatic (triplet).

View Article Online
DOI: 10.1039/C8CP07875K

Conclusions

Energetic consequences of two different types of dibenzo-fusion of pentalene, in singlet and triplet states, were examined by density functional calculations which well reproduced the experimental data. While [*a*,*f*]-type fusion destabilizes singlet state by 21.4 kcal/mol (open-shell) and 21.67 kcal/mol (closed-shell), it stabilizes triplet state by 10.8 kcal/mol, relative to the [*a*,*e*]-type fusion. These trends were rationalized by the decomposition of relative energies into contributions from electrostatic, orbital, dispersion and deformation energies, quantification of donor-acceptor interactions by NBO analysis and by the calculation of aromaticity indices, such as HOMA, FLU_{π} and $NICS(1)_{zz}$, as well as by the NICS-*XY*-scan procedure.

The π-electronic system was found to be the most important factor which regulates the singlet state energies. Thus, the larger π-electron delocalization, which is inherent for [*a*,*f*] topology and which significantly weakens the π-bonding energy, triggers the structural change ending in an *ortho*-quinoidal form of one benzene ring. In this way the π-system becomes less delocalized and π-bonding energy is increased. The subsequent Pauli repulsion relief leads to the equilibrium [*a*,*f*]-geometry, which is still characterized by weaker orbital interactions compared with [*a*,*e*]-DBP. They present the major source of energy difference between the isomers, the next important term being weaker electrostatic attractions. The driving force toward the diradical state of [*a*,*f*]-DBP is the recovery of the 6π-electron benzene subunit, though this has only slight stabilizing effect.

In the triplet state the two topologies stabilize the unpaired spin density in two different ways: over the central pentalene moiety for [*a*,*e*]-type fusion and over the central trimethylenemethane subunit for [*a*,*f*]-type fusion. The latter features smaller Pauli repulsion, stronger π-bonding and two aromatic benzene rings, which are the main reasons for the greater stability of [*a*,*f*]-DBP in the triplet state.

View Article Online
DOI: 10.1039/C8CP07875K

While benzene and pentalene subunits retain their local diatropicity and paratropicity in [*a*,*e*]-DBP, which only become weaker, the [*a*,*f*] topology results in large global paratropicity which involves benzene rings, as well. It is the most prominent in closed-shell C_{2v} symmetry structure and the least in C_s diradical state. In triplet state, both compounds sustain diatropic currents throughout the whole molecules. However, in [*a*,*e*]-DBP molecular perimeter takes up the largest currents, while in [*a*,*f*]-DBP they are more intense at benzene rings.

Acknowledgements

This work was supported by the Ministry of Education, Science and Technological Development of the Republic of Serbia, project No. 172020.

Conflicts of Interest

There are no conflicts to declare.

References

1. a) E. Hückel, *Z. Phys.*, 1931, **70**, 204-286; b) E. Hückel, *Z. Phys.*, 1931, **72**, 310-337; c) W. von E. Doering and F. L. Detert, *J. Am. Chem. Soc.*, 1951, **73**, 876-877.
2. a) R. Breslow, J. Brown and J. J. Gajewski, *J. Am. Chem. Soc.*, 1967, **89**, 4383-4390; b) R. Breslow, *Acc. Chem. Res.*, 1973, **6**, 393-398.
3. a) R. Breslow, *Pure Appl. Chem.*, 1971, **28**, 111-130; b) P. von R. Schleyer and H. Jiao, *Pure Appl. Chem.*, 1996, **68**, 209-218; c) R. H. Mitchell, *Chem. Rev.*, 2001, **101**, 1301-1316; d) K. B. Wiberg, *Chem. Rev.*, 2001, **101**, 1317-1331; e) J. A. N. F. Gomes and R. B. Mallion, *Chem. Rev.*, 2001, **101**, 1349-1383; M. Randić, *Chem. Rev.*, 2003, **103**, 3449-3605; f) Z. Chen. C. S. Wannere, C. Corminboeuf, R. Puchta and P. von R. Schleyer, *Chem. Rev.*, 2005, **105**, 3842-3888; g) T. Bally, *Angew. Chem. Int. Ed.*, 2006, **45**, 6616-6619; h) R. Islas,

T. Heine and G. Merino, *Acc. Chem. Res.*, 2012, **45**, 215-228; i) T. M. Krygowski, H. Szatylowicz, O. A. Stasyuk, J. Dominikowska and M. Palusiak, *Chem. Rev.*, 2014, **114**, 6383-6422; j) R. Breslow, *Chem. Rec.*, 2014, **14**, 1174-1182; k) R. Gershoni-Poranne and A. Stanger, *Chem. Soc. Rev.*, 2015, **44**, 6597-6615; l) F. Feixas, E. Matito, J. Poater and M. Solà, *Chem. Soc. Rev.*, 2015, **44**, 6434-6451.

4. T. Bally, S. Chai, M. Neuenschwander and Z. Zhu, *J. Am. Chem. Soc.*, 1997, **119**, 1869-1875.
5. O. T. Summerscales and F. G. N. Cloke, *Coord. Chem. Rev.*, 2006, **250**, 1122-1140.
6. T. Cai, L. Xu, C. Shu, J. E. Reid, H. W. Gibson and H. C. Dorn, *J. Phys. Chem. C*, 2008, **112**, 19203-19208.
7. H. Hopf, *Angew. Chem. Int. Ed.*, 2013, **52**, 12224-12226.
8. a) T. Kawase, T. Fijuwara, C. Kitamura, A. Konishi, Y. Hirao, K. Matsumoto, H. Kurata, T. Kubo, S. Shinamura, H. Mori, E. Miyazaki and K. Takimiya, *Angew. Chem. Int. Ed.*, 2010, **49**, 7728-7732; b) Z. U. Levi and T. D. Tilley, *J. Am. Chem. Soc.*, 2010, **132**, 11012-11014; c) X. Yin, Y. Li, Y. Zhu, Y. Kan, Y. Li and D. Zhu, *Org. Lett.*, 2011, **13**, 1520-1523; d) P. Rivera-Fuentes, M. von W. Rekowski, W. B. Schweizer, J.-P. Gisselbrecht, C. Boudon and F. Diederich, *Org. Lett.*, 2012, **14**, 4066-4069; e) G. London, M. von W. Rekowski, O. Dumele, W. B. Schweizer, J.-P. Gisselbrecht, C. Boudon and F. Diederich, *Chem. Sci.*, 2014, **5**, 965-972; f) G. Dai, J. Chang, W. Zhang, S. Bai, K.-W. Huang, J. Xu and C. Chi, *Chem. Comm.*, 2015, **51**, 503-506; g) M. Nakano, I. Osaka and K. Takimiya, *J. Mater. Chem. C*, 2015, **3**, 283-290.
9. K. Brand, *Ber. Detsch. Chem. Ges*., 1912, **45**, 3071-3077.
10. C. T. Blood and R. P. Linstead, *J. Chem. Soc*., 1952, 2263-2268.
11. a) P. W. Fowler, E. Steiner, R. W. A. Havenith and L. W. Jenneskens, *Magn. Reson. Chem.*, 2004, **42**, S68-S78; b) M. Dimitrova, H. Fliegl and D. Sundholm, *Phys. Chem. Chem. Phys.*, 2017, **19**, 20213-20223.

View Article Online
DOI: 10.1039/C8CP07875K

12. R. Ayub, O. El Bakouri, K. Jorner, M. Solà and H. Ottosson, *J. Org. Chem.*, 2017, **82**, 6327-6340.

13. a) Z. U. Levi and T. D. Tilley, *J. Am. Chem. Soc.*, 2009, **131**, 2796-2797; b) J. Zhao, K. Oniwa, N. Asao, Y. Yamamoto and T. Jin, *J. Am. Chem. Soc.*, 2013, **135**, 10222-10225; c) C. Chen, M. Harhausen, A. Fukuzawa, S. Yamaguchi, R. Fröhlich, C. D. Daniliuc, J. L. Petersen, G. Kehr and G. Erker, *Chem. Asian. J.*, 2014, **9**, 1671-1681; d) K. Takahashi, S. Ito, R. Shintani and K. Nozaki, *Chem. Sci.*, 2017, **8**, 101-107; e) J. Wilbuer, D. C. Grenz, G. Schnakenburg and B. Esser, *Org. Chem. Front.*, 2017, **4**, 658-663.

14. a) C. K. Frederickson, L. N. Zakharov and M. M. Haley, *J. Am. Chem. Soc.*, 2016, **138**, 16827-16838; b) H. Oshima, A. Fukazawa and S. Yamaguchi, *Angew. Chem. Int. Ed.*, 2017, **56**, 3270-3274.

15. a) S. J. Cristol, P. R. Whittle and A. R. Dahl, *J. Org. Chem.*, 1970, **35**, 3172-3174; b) T. Uyehara, T. Honda and Y. Kitahara, *Chem. Lett.*, 1977, 1233-1236; c) Y. A. Ustynyuk, O. I. Trifonova, Y. F. Oprunenko, V. I. Mstislavskiy, I. P. Gloriozov and N. A. Ustynyuk, *Organometallics*, 1990, **9**, 1707-1709.

16. A. Konishi, Y. Okada, M. Nakano, K. Sugisaki, K. Sato, T. Takui and M. Yasuda, *J. Am. Chem. Soc.*, 2017, **139**, 15284-15287.

17. a) T. Nakajima and A. Toyota, *Chem. Phys. Lett.*, 1969, **3**, 272-274; b) T. Nakajima, *Pure Appl. Chem.*, 1971, **28**, 219-238.

18. For selected examples, see: a) J. Poater, R. Visser, M. Solà and F. M. Bickelhaupt, *J. Org. Chem.*, 2007, **72**, 1134-1142; b) Y. Wang, J. I.-C. Wu, Q. Li and P. v. R. Schleyer, *Org. Lett.*, 2010, **12**, 4824-4827; c) M. El-Hamdi, W. Tiznado, J. Poater and M. Solà, *J. Org. Chem.*, 2011, **76**, 8913-8921; d) M. Contreras, E. Osorio, F. Ferraro, G. Puga, K. J. Donald, J. G. Harrison, G. Merino and W. Tiznado, *Chem. Eur. J.*, 2013, **19**, 2305-2310; e) M. Baranac-Stojanović, *Chem. Eur. J.*, 2014, **20**, 16558-16565; f) J. Cao, G. London, O.

Dumele, M. von Wantoch Rekowski, N. Trapp, L. Ruhlmann, C. Boudon, A. Stanger and F. Diederich, *J. Am. Chem. Soc.*, 2015, **137**, 7178-7188.

19. M. J. Frisch, G. W. Trucks, H. B. Schlegel, G. E. Scuseria, M. A. Robb, J. R. Cheeseman, G. Scalmani, V. Barone, B. Mennucci, G. A. Petersson, H. Nakatsuji, M. Caricato, X. Li, H. P. Hratchian, A. F. Izmaylov, J. Bloino, G. Zheng, J. L. Sonnenberg, M. Hada, M. Ehara, K. Toyota, R. Fukuda, J. Hasegawa, M. Ishida, T. Nakajima, Y. Honda, O. Kitao, H. Nakai, T. Vreven, J. A. Montgomery, Jr., J. E. Peralta, F. Ogliaro, M. Bearpark, J. J. Heyd, E. Brothers, K. N. Kudin, V. N. Staroverov, T. Keith, R. Kobayashi, J. Normand, K. Raghavachari, A. Rendell, J. C. Burant, S. S. Iyengar, J. Tomasi, M. Cossi, N. Rega, J. M. Millam, M. Klene, J. E. Knox, J. B. Cross, V. Bakken, C. Adamo, J. Jaramillo, R. Gomperts, R. E. Stratmann, O. Yazyev, A. J. Austin, R. Cammi, C. Pomelli, J. W. Ochterski, R. L. Martin, K. Morokuma, V. G. Zakrzewski, G. A. Voth, P. Salvador, J. J. Dannenberg, S. Dapprich, A. D. Daniels, O. Farkas, J. B. Foresman, J. V. Ortiz, J. Cioslowski and D. J. Fox, *Gaussian 09 (Revision D.01)*, Gaussian, Inc., Wallingford CT, 2013.
20. a) A. D. Becke, *J. Chem. Phys.*, 1993, **98**, 5648–5652; b) C. Lee, W. Yang and R. G. Parr, *Phys. Rev. B: Condens. Matter Mater. Phys.*, 1988, **37**, 785–789; c) J. B. Foresman and A. Frisch in *Exploring Chemistry with Electronic Structure Methods*, Gaussian, Inc., 1996.
21. a) M. Bendikov, H. M. Duong, K. Starkey, K. N. Houk, E. A. Carter and F. Wudi, *J. Am. Chem. Soc.*, 2004, **126**, 7416-7417; b) C. P. Constantinidies, P. A. Koutentis and J. Schatz, *J. Am. Chem. Soc.*, 2004, **126**, 16232-16241; c) S. Marković, J. Đurđević, S. Jeremić and I. Gutman, *J. Serb. Chem. Soc.*, 2010, **75**, 1241-1249; d) X. Gao, J. L. Hodgson, D.-e. Jiang, S. B. Zhang, S. Nagase, G. P. Miller and Z. Chen, *Org. Lett.*, 2011, **13**, 3316-3319; e) S. Radenković, M. Antić, J. Đurđević and S. Jeremić, *Monatsch. Chem.*, 2014, **145**, 281-290.
22. P. Su and H. Li, *J. Chem. Phys.*, 2009, **131**, 014102.
23. M. W. Schmidt, K. K. Baldridge, J. A. Boatz, S. T. Elbert, M. S. Gordon, J. H. Jensen, S. Koseki, N. Matsunaga, K. A. Nguyen, S. J. Su, T. L. Windus, M. Dupuis and J. A.

Montgomery, Jr., *J. Comput. Chem.*, 1993, **14**, 1347-1363; Gamess 2013-R1 version was used in this work.

View Article Online
DOI: 10.1039/C8CP07875K

24. a) T. M. Krygowski and M. K. Cyrański, *Chem. Rev.*, 2001, **101**, 1385-1419; b) J. Kruszewski and T. M. Krygowski, *Tetrahedron Lett.*, 1972, 3839-3842.

25. E. Matito, M. Duran and M. Solà, *J. Chem. Phys.*, 2005, **122**, 014109.

26. H. Fallah-Bagher-Shaidaei, C. S. Wannere, C. Corminboeuf, R. Puchta and P. v. R. Schleyer, *Org. Lett.*, 2006, **8**, 863-866.

27. T. Lu and F. Chen, *J. Comput. Chem.*, 2012, **33**, 580-592.

28. a) R. Ditchfeld, *Mol. Phys.*, 1974, **27**, 789-807; (b) K. Wolinski, J. F. Hinton and P. Pulay, *J. Am. Chem. Soc.*, 1990, **112**, 8251-8260.

29. a) A. Rahalkar and A. Stanger, Aroma. http://chemistry.technion.ac.il/members/amnon-stanger/; b) A. Stanger, *J. Org. Chem.*, 2006, **71**, 883-893; c) A. Stanger, *J. Org. Chem.*, 2010, **75**, 2281-2288; d) R. Gershoni-Poranne and A. Stanger, *Chem. Eur. J.*, 2014, **20**, 5673-5688.

30. a) E. D. Glendening, C. R. Landis and F. Weinhold, *WIREs Comput. Mol. Sci.*, 2012, **2**, 1-42; b) F. Weinhold and C. R. Landis, in *Discovering Chemistry with Natural Bond Orbitals*, John Wiley & Sons, Inc., 2012.

31. E. D. Glendening, J. K. Badenhoop, A. E. Reed, J. E. Carpenter, J. A. Bohmann, C. M. Morales, C. R. Landis and F. Weinhold, NBO 6.0, Theoretical Chemistry Institute, University of Wisconsin, Madison, WI, 2013.

32. Y. Mo and P. v. R. Schleyer, *Chem. Eur. J.*, 2006, **12**, 2009-2020.

33. The original labeling of ref. 22 was changed so that electrostatic energy is labeled, herein, as ΔE_{elstat} (originally ΔE_{es}) and stabilizing orbital interaction energy is labeled, herein, as ΔE_{oi} (originally ΔE_{pol}). The LMOEDA provides separately exchange and repulsion energies (ΔE_{ex} and ΔE_{rep}, respectively), which were summed to represent the Pauli repulsion energy component, labeled as ΔE_{Pauli}.

View Article Online
DOI: 10.1039/C8CP07875K

34. A comprehensive analysis of aromatic benzene and antiaromatic cyclobutadiene revealed that the π-electron system is more stable when it is localized and, thus, always favours localization against the delocalizing force of σ-electrons. This π-electron tendency is much more pronounced in antiaromatic compound resulting in the lower symmetry localized molecule. See: S. C. A. H. Pierrefixe and F. M. Bickelhaupt, *Chem. Eur. J.*, 2007, **13**, 6321-6328.

35. Z. Zeng, X. Shi, C. Chi, J. T. López Navarrete, J. Casado and J. Wu, *Chem. Soc. Rev.*, 2015, **44**, 6578-6596.

36. a) N. C. Baird, *J. Am. Chem. Soc.*, 1972, **94**, 4941-4948; b) P. Karadakov, *J. Phys. Chem. A*, 2008, **112**, 7303-7309; c) P. Karadakov, P. Hearnshaw and K. E. Horner, *J. Org. Chem.*, 2016, **81**, 11346-11352; d) M. Rosenberg, C. Dahlstrand, K. Kilså and H. Ottosson, *Chem. Rev.*, 2014, **114**, 5379-5425; e) R. Papadakis and H. Ottosson, *Chem. Soc. Rev.*, 2015, **44**, 6472-6493.

TOC graphic

View Article Online
DOI: 10.1039/C8CP07875K

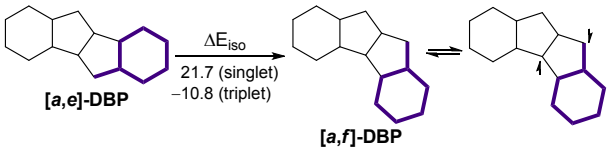

singlet: locally diatropic and paratropic [*a*,e], globally paratropic [*a*,f]
triplet: globally diatropic [*a*,e], globally and locally diatropic [*a*,f]

DFT calculations provided an insight into factors responsible for energy trend of the two isomeric dibenzopentalenes and types of magnetically induced currents.